

A molecular dynamics study of the effects of fast molecular motions on solid-state NMR parameters

Martin Dračinský,^{a,b,*} Paul Hodgkinson^{a,*}

^a*Department of Chemistry, Durham University, South Road, DH1 3LE, Durham, UK*

^b*Institute of Organic Chemistry and Biochemistry, Flemingovo nám. 2, 16610, Prague, Czech Republic*

Abstract

The influence of fast molecular motions on NMR parameters in molecular organic solids is explored on a set of amino acids and nucleic acid bases. A combination of DFT molecular dynamics and calculations of shielding and electric field gradient (EFG) tensors reveals the impact of vibrational motions on isotropic chemical shifts, chemical shift anisotropies (CSAs) and quadrupolar interactions. We demonstrate that molecular motion has a significant effect on average molecular structures, and that neglecting the effects of motion on crystal structures derived by diffraction methods may lead to significant errors of calculated isotropic chemical shifts. Re-orientation of the NMR tensors by molecular motion reduces the magnitudes of the NMR anisotropies, and inclusion of molecular dynamics can significantly improve the agreement between calculated quadrupolar couplings and experimental values.

Introduction

It is well established that fast molecular motions, such as vibrations, conformational averaging, molecular aggregation, will average NMR parameters.^{1,2} Isotope shifts³ and the temperature dependence of NMR parameters are experimental manifestations of such dynamic averaging effects. In the last decade, the gauge-including projector-augmented wave (GIPAW) procedure has been developed for the prediction of the magnetic resonance parameters in solids.⁴ The power of the GIPAW approach for calculating NMR properties for fully periodic crystal structures, specifically in the context of organic solids, has been well documented;^{1, 5-6} Such quantum chemical calculations are typically performed using static structures, i.e. at 0 K and neglecting zero-point motion, and dynamics can lead to significant discrepancies between computed and experimental data. In solutions, where the configurations of neighbours change dynamically, the intermolecular contributions to shielding also change with changing configurations.^{2, 7} Therefore, dynamic averaging needs to be taken into account, even when there are no significant strong intermolecular interactions such as hydrogen bonding.

In the solid state, local dynamics will average the NMR tensor parameters such as the CSA, dipolar interactions and quadrupolar interactions, leading to discrepancies between calculated data and experimental measurements (which are usually performed at ambient temperature). Various scaling methods have been proposed to bring computed and experimental values in line. For example, least-squares fitting of calculated vs. experimental quadrupolar couplings has been used to determine scaling factors for individual nuclei in a test set of compounds.⁸ Interestingly, the smallest scaling factor (0.85) was found for the lightest isotope in the test set, ¹¹B and, within the error, a monotonic decrease with increasing atom number was found with the scaling very close to 1 for ²⁷Al. Although the overestimation of the calculated quadrupolar couplings was ascribed to systematic

deficiencies of the DFT calculations, the mass dependence of the scaling factor suggests that molecular motion may at least partially explain the discrepancies between experimental and calculated data. Chemical shift anisotropies have also often been found to be overestimated by DFT calculations and several scaling factors ranging from 0.76 to 0.95 and depending on the studied structures have been proposed, as summarised in ref.⁹ If the discrepancies between calculated and experimental data lie at least partially in the neglect of the dynamics in the calculations, then scaling removes potential information about dynamics. Understanding how fast dynamics affects NMR tensor parameters may lead not only to a better agreement with experiment but also to a proper description of the dynamics in the systems studied.

Diffraction experiments are also affected by molecular motions. In conventional Bragg diffraction studies, the interatomic distance between two sites A and B is assumed to correspond to the distance between the centres of thermal ellipsoids, $d_0 = |\langle r_A \rangle - \langle r_B \rangle|$, where $\langle r_A \rangle$ and $\langle r_B \rangle$ are the individual positions averaged over any disorder (which is here assumed to be purely dynamic in nature). This equivalence is only strictly true if there is no correlation between the instantaneous deviations of the atomic positions from the average structure. This distance d_0 may differ substantially from the instantaneous interatomic distance averaged over time, $d = \langle |r_A - r_B| \rangle$.¹⁰ As the amplitudes of molecular motion increase with temperature, the apparent distances d_0 become shorter. Since NMR parameters depend on the instantaneous molecular geometry, calculation of NMR data using single structures determined by diffraction may thus introduce an error dependent on the temperature of the diffraction experiment.

Large-amplitude motions in solids, e.g. the dynamics of methyl groups and other small molecular fragments, are frequently studied by NMR,¹¹⁻¹³ and a number of studies have explained the discrepancies between experimental and calculated tensors in such terms e.g. ³¹P tensors in phenylphosphonic acid,¹⁴ rotational dynamics of sulfonic acids by variable temperature ¹⁷O NMR,¹⁵ or local dynamics in silica-encapsulated liposomes.¹⁶ Fast, small-amplitude motions have a much more subtle effect on NMR parameters. Here molecular dynamics (MD) or Monte Carlo simulations provide a general approach for determining how NMR parameters, including relaxation times,¹⁷ are affected by motion. Both DFT and molecular mechanics simulations can be used. DFT simulations provide more realistic internuclear forces (and therefore the time evolution of the dynamic system) than can be estimated by any empirical force field. Furthermore, DFT-MD allows for anharmonic vibrations, whereas most of the current molecular mechanics force fields are based on harmonic approximation. The computational cost of DFT molecular dynamics only allows the simulation of trajectories over several tens of picoseconds for systems of a modest size, but this is sufficient for capturing fast vibrational motions. On the other hand, molecular dynamics based on empirical force fields are more appropriate for studying extended systems such as biomacromolecules, and longer nano- to micro-second time scales.

Another approach for addressing vibrational motion in solids relies on the calculation of vibrational wave function with the vibrational configuration interaction or other simplified quantum anharmonic schemes.¹⁸⁻¹⁹ This method is computationally demanding and many approximations have to be adopted in practical computations, in particular for the treatment of the variation of the shielding with vibrational coordinates. However, the results confirmed an important vibrational

contribution (up to almost 10 ppm for nitrogen atom) to isotropic chemical shifts, which was in qualitative agreement with the results of DFT-MD.

In the context of NMR, the vast majority of the reported molecular dynamics studies have concentrated on the time averaging of isotropic chemical shift only. The averaging of calculated chemical shifts usually leads to a significant improvement of the agreement between calculated and experimental data.^{7, 20-24} To the best of our knowledge, only few examples of full tensor averaging have been reported. ⁵¹V NMR parameters of solid VOCl₃ were calculated by a combination of Car-Parrinello molecular dynamics with embedded cluster NMR calculations.²⁵ Only minor changes were observed for vanadium isotropic shielding and shielding anisotropies, whereas the quadrupolar coupling was reduced significantly by the MD averaging, resulting in a better agreement with the experimental value. Water dynamics were studied by Pennanen et al.²⁶ Both chemical shifts and EFG tensors were calculated for geometry snapshots from Car-Parrinello molecular dynamics of water in the liquid and gaseous states. The averaged tensors were used to calculate the gas-to-liquid chemical shift change as well as the corresponding change in the nuclear quadrupole coupling of ¹⁷O and ²H.

Here we explore the influence of fast molecular motions on the average molecular geometry, isotropic shielding, chemical shift anisotropy and nuclear quadrupolar interactions. We demonstrate that molecular vibrations / librations have an important and experimentally observable influence primarily on isotropic chemical shifts and quadrupolar couplings.

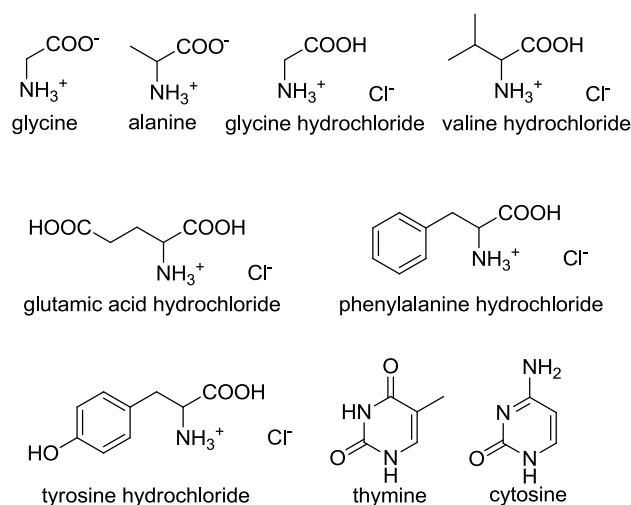


Figure 1. The studied set of model amino acids, amino acids hydrochlorides and nucleic acids bases.

Methods

Figure 1 shows the set of model amino acids, amino acids hydrochlorides and nucleic acids bases used. These were selected based on the availability of high-quality crystal structures and experimental NMR parameters. The atomic coordinates for glycine (GLYCIN20), alanine (LALNIN12), glycine hydrochloride (GLYHCL), valine hydrochloride (VALEHC11), glutamic acid hydrochloride (LGLUTA), phenylalanine hydrochloride (PHALNC01), tyrosine hydrochloride (LYRHC10), cytosine (CYTSIN01), and thymine (THYMIN01) were derived from the Cambridge Crystallographic Database.²⁷ Where available, neutron diffraction structures were used, since even hydrogen atoms are

accurately located by neutron diffraction²⁸ (in contrast to X-ray diffraction). The neutron diffraction structures were used without optimization of the atomic coordinates for calculations of static NMR parameters. In the case of cytosine and thymine, neutron data was unavailable, and X-ray structures were used after the positions of the hydrogen atoms had been optimised. Note that for consistency all crystal structures used in this work were determined at room temperature.

The NMR tensors of the infinite crystals were calculated by the CASTEP program,²⁹ which is a DFT-based code. Electron-correlation effects were modeled using the generalized gradient approximation of Perdew, Burke, and Ernzerhof.³⁰ For the hydrogen position optimization, we employed ‘on-the-fly’ pseudopotentials, a planewave cutoff energy of 600 eV with integrals taken over the Brillouin zone using a Monkhorst-Pack³¹ grid of a minimum k-point sampling of 0.05 \AA^{-1} . The NMR calculations were performed using the GIPAW approach^{4, 32} at a larger cutoff of 900 eV. These parameters calculated from the initial diffraction-derived structures are referred to as the “static diffraction” NMR parameters. These are reported using CASTEP’s definitions, which generally follow standard NMR practice,¹¹ except that the shielding anisotropy is defined as $\Delta\sigma = \sigma_{zz} - \frac{1}{2}(\sigma_{xx} + \sigma_{yy})$ rather than the more usual $\zeta = \sigma_{zz} - \sigma_{iso}$ (with $\zeta = 2 \Delta\sigma/3$).

Born-Oppenheimer molecular dynamics (BOMD) simulations were run in CASTEP using an *NVT* ensemble maintained at a constant temperature of 300 K using a Langevin thermostat, a 0.5 fs integration time step, ultrasoft pseudopotentials,³³ a planewave cutoff energy of 300 eV, and with integrals taken over the Brillouin zone using a Monkhorst-Pack³¹ grid of a minimum k-point sampling of 0.1 \AA^{-1} . The MD parameters were tested with respect to the convergence of atomic forces; an increase of the cutoff energy or k-point sampling led to changes in the calculated forces lower than 0.1 eV/\AA . For comparison, we also performed the MD simulation of glycine hydrochloride with ‘on the fly’ pseudopotentials and cutoff energy of 400 eV, but the resulting MD-induced changes of NMR parameters were close to the ultrasoft/300 eV approach (chemical shift differences lower than 1 ppm), while the calculation time was longer by 50%.

Optimisation of positions of all atoms is a prerequisite for molecular dynamics simulations otherwise the excess potential energy would transform to kinetic energy and the simulation would be unstable or longer equilibration would be necessary. The atomic positions were optimized at the same computational level prior to the MD runs leading to “MD-optimised structures”. The lattice parameters were fixed to the experimental values, and no dispersion corrections were required to maintain cell volumes during the MD simulations. It has been shown that dispersion correction did not significantly affect the calculated shieldings of solid glycine when the lattice parameters were fixed during geometry optimization in ref.¹⁹, in which the temperature dependence of the chemical shifts was studied. The center of mass was fixed to ensure that the random initial velocities did not result in translational motion. No symmetry constraints were applied during the runs as these are only relevant to the time-averaged structure. Simulation runs of 5 ps were performed for every compound.

In order to determine time-averaged NMR parameters, 41 geometries were selected at 1.0, 1.1, 1.2 ... 5.0 ps of each run for the NMR calculations. The unit cells contained two or four crystallographically equivalent molecules ($Z = 2$ or 4); therefore, 82 or 164 values were averaged for every chemically equivalent site. Where methyl group rotation occurred during the MD simulation,

averaging of the atomic positions leads to unrealistic geometries. Therefore, the methyl hydrogen positions were optimised for these structures before the calculation of NMR parameters. Averaged principal components of CSA and EFG tensors were obtained by averaging each tensor element for a tensor expressed in a fixed Cartesian frame and then diagonalising the average tensor matrix. The MD-induced change of each NMR parameter was then calculated as the difference between the averaged NMR parameters and those calculated on the structure where the positions of all atoms during the MD simulation were averaged ("MD-averaged structure"). For α -glycine, we constructed another structure where all interatomic distances in the MD-optimised structure were manually set to the interatomic distances $\langle |r_A - r_B| \rangle$ averaged over the whole MD trajectory ("adjusted-bond-length structure"). Where required for comparison with experimental data, NMR parameters incorporating the effects of motion were calculated as the static data (neutron or X-ray) plus the MD-induced change, e.g. $\sigma_{\text{iso}} = \sigma_{\text{iso}}(\text{static}) + \Delta\sigma_{\text{iso}}$ etc. This procedure takes advantage of cancellation of errors introduced by imperfect geometry optimisation because the MD-induced changes are calculated as the difference between the NMR parameter averaged over the DFT molecular dynamics and that calculated for the "MD-averaged structure". Hence any systematic error in the DFT-refined geometries is largely cancelled out in determining the MD-induced change.

Results

The influence of molecular dynamics on the apparent geometry

Apart from methyl group rotation observed in the case of thymine and alanine, no larger scale motions (e.g. conformational changes) were observed in the course of the MD runs. This is expected given the short time-scales being probed. The space explored by the nuclei of α -glycine and glycine hydrochloride during the MD simulation is shown in Figure S1 in the SI. The probability distributions of the bond distances during the MD simulation of α -glycine are depicted in Figure 2. It can be seen that the distribution of the carbon-oxygen bond distances is narrower and more symmetric than the other distributions, which is in agreement with the higher bond order in the COO^- group with delocalised negative charge. Some distance distributions, such as those for the C-C and N-H bonds, are noticeably asymmetric, but this does not obviously correlate with the extent to which these bonds increase in length with increasing temperature (cf. Table 1).

As observed in Table 1, all interatomic distances become slightly shorter in comparison with the optimised structures when the atomic positions are averaged over the whole MD trajectories ("MD-averaged structure", see Table 1). These effective distances are directly comparable with the interatomic distances obtained by diffraction methods at the same temperature because both include the effect of temperature on the apparent bond distances. The differences between the MD-averaged and the diffraction geometry may be ascribed to the limitations of the DFT method (including the choice of the pseudopotentials and basis set) as well as any experimental errors. For α -glycine the root mean square deviation (RMSD) between the diffraction and the MD-averaged structures is 1.2 pm. Solid α -glycine has been studied by diffraction methods at various temperatures and the apparent decrease of bond distances with increasing temperature is reported in the Table 1. In the case of the α -glycine system, bond distances corrected for molecular motion at room temperature have been reported.³⁴ These are significantly larger than the bond distances observed at 23 K (see columns 2 and 5 in Table 1). Note however, that the rigid-body model used is a

drastic approximation, which ignores internal vibrational modes.¹⁰ Similarly, we obtained longer MD-averaged instantaneous distances $\langle |r_A - r_B| \rangle$ of the covalent bonds in α -glycine than in either the MD-optimised structure (i.e. at 0 K without zero-point vibrational motion) or the structure with MD-averaged atomic positions $|\langle r_A \rangle - \langle r_B \rangle|$.

The differences in bond lengths have a significant impact on the NMR parameters. This is documented in Table 2, which shows the isotropic shielding values of solid α -glycine calculated for various geometries. As discussed above, the neutron structure acquired at 300 K is the single structure that is most directly comparable with that obtained by averaging the atomic positions over the MD run. In agreement with this, the isotropic shielding values calculated for the neutron structures were closest to the values obtained for the structures with the MD-averaged atomic positions (for α -glycine compare Columns 2 and 4 in Table 2), although some significant differences in calculated shielding values are observed (e.g. carbon atom C1 and oxygen atoms).

MD-averaged isotropic shieldings were obtained as the average of the shieldings calculated on 41 geometry snapshots from MD simulations. A reasonable convergence of the calculated isotropic shieldings (changes lower than 1 ppm for ^{13}C and ^{15}N) was usually achieved after the averaging of 20-30 geometries. This convergence is thus much faster than when calculating NMR parameters of compounds in solution, where the rapid fluctuation of the solvent molecules requires the averaging of several hundreds or thousands MD snapshots to obtain reasonably converged chemical shifts.³⁵ The snapshot-averaged shieldings are closest to those obtained for the single structure where the bond distances were set manually to the average bond distances (“adjusted-bond-length structure”, $\langle |r_A - r_B| \rangle$) during the MD simulation (last two columns in the Table 2). Therefore, the static calculation on the ‘adjusted-bond-length geometry’ may provide a rough estimate of the vibrational effect on the isotropic shieldings. This is not, however, true for chemical shift anisotropies and quadrupolar couplings as shown below.

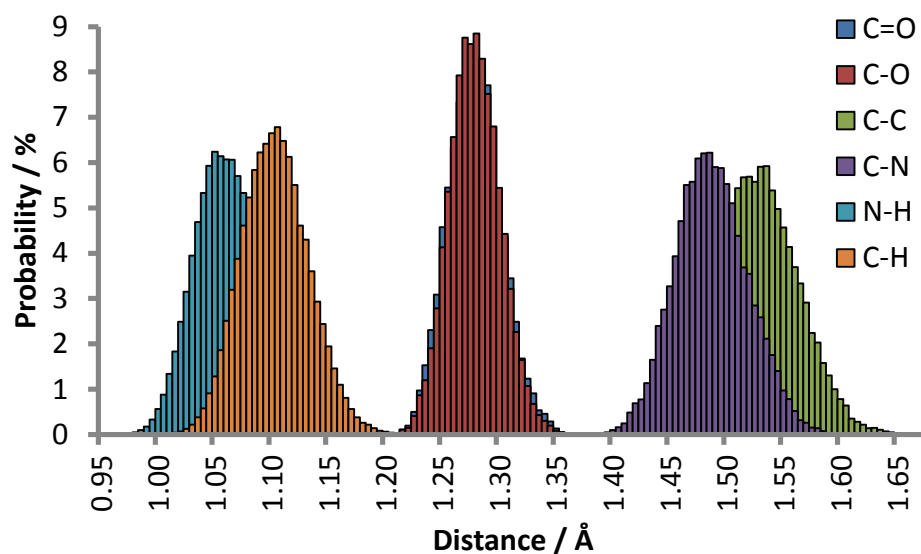


Figure 2. The probability distribution of bond distances in α -glycine during the MD simulation at 300 K sampled by 0.005 Å.

Table 1. Interatomic distances (in angstroms) in solid α -glycine.

distance	X-Ray ^a (<i>T</i> = 23 K)	Neutron ^b (<i>T</i> = 301 K)	Neutron ^b (<i>T</i> = 427 K)	Neutron ^c r.t.	Optimised ^d (<i>T</i> = 0 K)	MD-averaged ^e (<i>T</i> = 300 K)	Adjusted- bond-length ^f (<i>T</i> = 300 K)
C=O	1.258	1.248	1.237	1.261	1.272	1.267	1.276
C-O	1.261	1.251	1.253	1.261	1.277	1.269	1.276
C-C	1.527	1.525	1.521	1.539	1.523	1.520	1.528
C-N	1.482	1.474	1.473	1.490	1.479	1.478	1.485
C _α -H		1.090	1.079	1.097	1.097	1.089	1.101
N-H		1.042	1.027	1.046	1.059	1.053	1.064

^aData from ref.³⁶ Distances to hydrogen atoms are not reported since they are poorly estimated by XRD. ^bData from ref.³⁷ ^cDistances corrected for rigid-body motion.³⁴ ^dGeometry optimised at the same computational level used for the molecular dynamics (see Methods). ^eDistances between averaged atomic positions $|\langle r_A \rangle - \langle r_B \rangle|$. ^fAverage interatomic distances $\langle |r_A - r_B| \rangle$.

Table 2. The calculated isotropic shielding values (in ppm) for various geometries of solid α -glycine, and the RMS deviation from the neutron structure values.

atom	Neutron (<i>T</i> = 300 K)	Optimised ^a (<i>T</i> = 0 K)	MD-averaged ^b (<i>T</i> = 300 K)	Adjusted-bond- length ^c (<i>T</i> = 300 K)	MD snapshots ^d (<i>T</i> = 300 K)
C1	-4.97	-13.28	-10.69	-13.97	-13.54
C2	130.49	128.49	130.50	127.23	126.49
N	194.54	191.98	193.80	190.36	189.07
O1	-35.56	-56.66	-47.81	-57.85	-59.63
O2	-24.32	-44.20	-41.08	-45.96	-52.79
H _α	26.73	26.48	26.68	26.33	25.92
H _{α'}	27.79	27.51	27.90	27.41	27.34
NH ₃	22.39	21.26	21.63	21.05	21.30
<i>RMSD</i>		10.7	7.6	11.6	13.7

^aGeometry optimised at the same computational level used for the molecular dynamics (see Methods). ^bMD-averaged atomic positions. ^cGeometry optimised structure with all bond distances manually set to average interatomic distances during MD. ^dAveraged shielding values calculated for 41 geometry snapshots from the MD simulation.

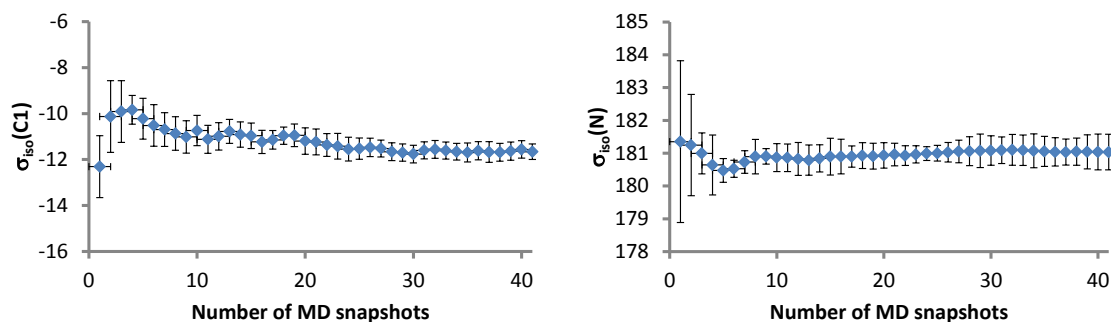


Figure 3. The convergence of the isotropic shieldings for the carbonyl carbon (left) and nitrogen atom (right) in glycine hydrochloride with respect to the number of MD geometry snapshots used in the cumulative average. The shielding values for the four equivalent molecules in the unit cell were averaged independently and the error bars were estimated as the standard error of this set of four values with respect to their mean.

Averaging of NMR parameters over the MD trajectories: chemical shifts

The MD-induced changes in isotropic shielding values of all nuclei in the studied series of compounds were usually negative. There are, however, significant differences between the average MD-induced changes for different nuclei; the smallest average change was found for hydrogens (-0.5 ± 0.36 ppm) followed by carbon (-3.8 ± 1.4 ppm), nitrogen (-6.7 ± 2.4 ppm), oxygen (-13.7 ± 3.7 ppm), and chlorine atoms (-18.9 ± 3.1 ppm). These different changes largely reflect the different chemical shift ranges of these nuclei, which span from 20 ppm for hydrogens to 200 ppm for carbons and several hundreds to thousands of ppm for nitrogen, oxygen and chlorine atoms. Note that ^1H chemical shift difference between zero and 300 K of 0.3 – 0.5 ppm were found experimentally when extrapolating variable temperature data.³⁸ As an example, calculated static isotropic shieldings and differences in the shieldings caused by molecular dynamics (MD-induced changes) for glycine hydrochloride are shown in Table 3.

Table 3. NMR parameters of glycine hydrochloride calculated from the neutron structure, and the changes of the parameters upon averaging over MD simulation. The numbers in parenthesis were obtained by averaging the calculated values of $\Delta\sigma$ and $\Delta\chi$ rather than full tensor averaging followed by diagonalisation.

	σ_{iso} / ppm	$\Delta\sigma_{\text{iso}}$ / ppm	$\Delta\sigma$ / ppm	$\Delta\Delta\sigma$ / ppm	η	$\Delta\eta$	χ / MHz	$\Delta\chi$ / MHz	η_{α}	$\Delta\eta_{\alpha}$
NH ₃	22.50	-0.99	24.12	-1.19(-0.54)	0.19	-0.01	0.20	-0.03(-0.02)	0.03	0.00
OH	17.83	-0.37	28.72	-1.49(-1.05)	0.07	0.02	0.21	-0.01(-0.01)	0.09	-0.01
H α	26.69	-1.14	7.78	-0.72(-0.17)	0.38	-0.06	0.19	-0.03(-0.02)	0.09	-0.01
H α	25.66	-1.12	9.54	-0.48(0.25)	0.50	-0.01	0.19	-0.03(-0.02)	0.08	-0.01
COO	-2.82	-4.16	-135.73	2.28(0.34)	0.50	0.01	-	-	-	-
CH ₂	132.34	-6.04	35.96	-2.12(-0.24)	0.35	-0.05	-	-	-	-
N	191.45	-8.62	13.23	-0.12(5.16)	0.25	0.13	1.27	-0.01(0.07)	0.14	-0.02
=O	-63.19	-13.93	524.97	-14.39(4.23)	0.42	-0.01	8.53	-0.14(0.06)	0.04	0.04
-OH	78.64	-11.92	-242.91	0.19(7.34)	0.12	-0.01	-7.69	0.17(0.00)	0.23	0.01
Cl	885.22	-14.12	90.69	-1.85(5.76)	0.67	0.00	-8.14	0.43(0.32)	0.80	0.01

The influence of molecular dynamics on chemical shift anisotropies can be divided into two contributions. First, the molecular motion has a direct impact on the instantaneous magnitudes of the CSAs and second, the orientation of the CSA tensors can also change, which leads to more spherical averaged tensors (see Figure S2 for a graphical representation). The first contribution can be estimated by averaging the calculated values of the CSAs during the MD (numbers in parenthesis in the Table 3), while the overall influence of molecular motion on the CSA is obtained by averaging the full shielding tensor and calculating the CSA from the eigenvalues of the average tensor. The influence of the shielding tensor reorientation is then reflected in difference between these two measures. The sign of the first contribution is dependent on the local environment, while the re-orientation component always decreases the magnitude of the anisotropy. The fact the molecular dynamics averaging leads typically to lower absolute values of the CSAs, which is consistent with the experimental observations discussed earlier, implies that re-orientation is generally the most significant factor. This in turn implies that the discrepancy between experimental and calculated CSAs is expected to approximately correlate with the degree of re-orientational motion, even though the overall connection is complicated by local electronic factors.

To put the effects of tensor reorientation in more geometric terms, we calculated the projections of normalised CSA eigenvectors calculated for the MD geometry snapshots onto the CSA eigenvectors calculated for the MD-optimised structure (i.e., $\cos \beta$, where β is the angle between the principal axis components of the CSA tensor in the reference optimised structure and in a MD geometry snapshot). Typically, the average projections were higher than 0.97; the corresponding average reorientation angles β of the CSA tensors were usually in the range 4–14 degrees with a slightly larger fluctuation of the CSA tensors of the central atoms of CH₃ and NH₃ groups with the average reorientation angle of 19° for C atoms and 25° for N.

The overall MD-induced changes of the CSAs were usually rather small and close to the experimental error in determining CSAs (a few ppm) for hydrogen, carbon and nitrogen atoms. For glycine and alanine the calculated CSAs are very close to the experimental values reported previously.³⁹ This good agreement of the calculated and experimental CSAs appears to contradict the scaling of calculated CSA values proposed previously for ¹³C chemical shift anisotropies of disaccharides with

reported scaling factors as low as 0.75.⁹ However, the principal axis components of carbon chemical shift tensor of sucrose were reported three times previously and the span of the reported experimental anisotropies acquired at room temperature is rather large (for example for C1 the CSA values were 21.8, 23.7, and 29.8 ppm respectively),^{9, 40-41} which reflects the difficulty in the measurement of small CSA values. The scaling factor of 0.75 was proposed in ref.⁹ on the basis of experimental CSA values that were consistently lower than in ref.⁴⁰

Larger MD-induced changes of the CSAs were observed for oxygen and chlorine atoms, but the measurement of CSAs in the presence of significant quadrupolar interactions is experimentally demanding and the reported values usually have much higher error bars (tens of ppm). The asymmetry of the MD-averaged CSA tensors was usually close to the static calculations, and so the shape of the signals is not a particularly useful metric for this type of motion.

Averaging of NMR parameters over the MD trajectories: quadrupolar couplings

The absolute values of quadrupolar couplings were always lowered by the molecular dynamics averaging. Again, the reason for this lowering is the reorientation of the EFG tensors in the course of the dynamics. The average re-orientation angles of the EFG tensors during the MD were similar to those of the CSA tensors, and in the range of 6–10° with slightly larger fluctuations of the chloride anion EFG tensors. The absolute values of the quadrupolar couplings were lowered by 2–5%. For ²H and ¹⁴N nuclei, where the quadrupolar coupling is small, the MD-induced changes of the couplings were in the order of tens of kHz and the changes for ¹⁷O and ³⁵Cl nuclei were up to 0.3 MHz.

The experimental and calculated ¹⁷O quadrupolar couplings for all compounds in this study with available experimental data are summarised in Table 4. It can be clearly seen that including the effects of fast dynamics on the calculated couplings significantly improves agreement with experimental values. Therefore, we can conclude that the previously observed overestimation of the calculated ¹⁷O quadrupolar couplings was mainly caused by neglecting fast molecular motion in the static calculations. Note that static calculations performed on geometry optimized structures provide even larger absolute average deviations (0.41 MHz) from the experimental values than the calculations with the diffraction structures. The largest difference between the calculated and experimental data was found for the oxygen atom O2 in cytosine and oxygen atom O4 in thymine. However, the experimental spectrum used for the determination of this coupling⁴² was very noisy and the reported experimental error is probably underestimated; furthermore, the reported crystal structure of cytosine was published in 1973 and may not be sufficiently accurate. In contrast, some calculated chlorine quadrupolar couplings for the amino acid hydrochlorides systems studied were far from the experimental values, even after including the effects of molecular dynamics. The discrepancy between the calculated and experimental ³⁵Cl quadrupolar couplings was noted previously and in an effort to determine the cause of the discrepancy, the EFGs of some covalently bonded chlorine in organic compounds were calculated. The values were found to be in satisfying agreement with experiment and it was proposed that the differences in quadrupolar couplings for the amino acid hydrochlorides is possibly due to mobility effects of the anion.¹⁴ Here, we observe that fast motions cannot explain the discrepancy and we suspect that it is due to large scale motion of the chloride anion, which will be discussed in a separate paper.

Table 4. ^{17}O quadrupolar couplings (in MHz) calculated on static structures and with the inclusion of dynamics, average re-orientation angle β of the EFG tensor during the MD, and experimental quadrupolar couplings.

Compound	O site	CSD	CSD+MD	$\beta / ^\circ$	Exp	Ref.
Glycine HCl	O1	8.53	8.38	6	8.40±0.05	43
	O2	-7.69	-7.51	6	7.60±0.05	
Valine HCl	O1	8.59	8.41	7	8.40±0.05	43
	O2	-7.60	-7.45	6	7.35±0.05	
Phenylalanine HCl	O1	8.62	8.65	7	8.54±0.05	43
	O2	-7.79	-7.56	7	7.46±0.05	
Tyrosine HCl	O1	8.40	8.38	10	8.22±0.05	43
	O2	-7.37	-7.31	10	7.35±0.05	
	O3	8.82	-8.72	7	8.56±0.05	
Glutamic acid HCl ^a	O1	-7.41	-7.33	7	7.45±0.05	44
	O2	8.40	8.40	7	8.16±0.05	
	O3	8.62	8.44	7	8.31±0.05	
	O4	-7.86	-7.64	7	7.49±0.05	
Alanine	O1	8.32	8.19	6	7.86±0.1	14
	O2	6.81	6.83	8	6.53±0.1	
Cytosine	O2	7.72	7.68	6	7.20±0.05	42
Thymine	O2	6.96	6.88	15	6.65±0.05	42
	O4	9.08	8.96	6	8.40±0.05	
<i>AAD^b / MHz</i>		<i>0.26</i>	<i>0.18</i>			

^aData calculated for LGLUTA structure with optimised position of O4-H hydrogen atom. ^bAverage absolute deviation.

In the case of glutamic acid hydrochloride a much larger discrepancy was noted for one particular oxygen (O4). As discussed in detail in the SI, the calculated force on the hydrogen atom attached to the oxygen atom O4 is rather high (1.22 eV/Å), and optimising the position of this hydrogen atom improved the agreement with experiment considerably.

Conclusions

Using a series of model compounds, we have evaluated the importance of fast molecular motion on NMR isotropic shielding, chemical shift anisotropy and quadrupolar interactions. Atomic motions lead to apparent shortening of interatomic distances observed by diffraction, even though actual bond distances tend to increase slightly with increasing temperature. These effects are well-known within the diffraction community, but have not been addressed directly in NMR crystallography. As NMR is very sensitive to geometry, care must be taken when analysing NMR data calculated on crystal structures without a correction for the atomic motion, especially when the diffraction data was acquired at elevated temperatures (as is typically the case in neutron diffraction studies). Using diffraction structures obtained at ambient temperature with average atomic positions may lead to an error of several tenths of ppm for hydrogen nuclei and several ppm for other nuclei. Fortunately, these changes have a consistent sign and similar magnitudes for a given isotope. Therefore, the effects of fast motions on structures derived from diffraction are not expected to change

significantly the relative positioning of signals in calculated NMR spectra, and only (further) complicates the question of referencing the chemical shift scale. However, one should be careful when comparing calculated NMR data for two crystal structures determined at different temperatures. In these structures, the extent of the error will vary and optimisation of all atomic positions prior to the NMR calculation would be probably good practice.

For anisotropic interactions, such as the CSA and EFG, the reorientation of tensors during the motion leads to more spherical tensors, i.e. lower magnitude of chemical shift anisotropies and quadrupolar couplings. The average re-orientation angle of the NMR tensors is 5–25°. The changes of chemical shift anisotropies and quadrupolar couplings induced by the dynamics are in the order of few per cent and in the case of CSAs and quadrupolar couplings of hydrogen and nitrogen atoms, the induced changes are rather small. However, the changes of quadrupolar couplings of the nuclei with higher quadrupole moment (e.g. oxygen) are in the order of several hundreds of kHz. Therefore, vibrational averaging of quadrupolar couplings is needed when highly accurate predictions of the couplings are desired.

Acknowledgement

The research leading to these results has received funding from the People Programme (Marie Curie Actions) of the European Union's Seventh Framework Programme (FP7/2007-2013) under REA grant agreement n° 299242.

Supporting information

Electronic supplementary information (ESI) available: Calculated NMR parameters and further computational details.

References

1. Bonhomme, C.; Gervais, C.; Babonneau, F.; Coelho, C.; Pourpoint, F.; Azais, T.; Ashbrook, S. E.; Griffin, J. M.; Yates, J. R.; Mauri, F.; Pickard, C. J., *Chem. Rev.*, 2012, **112**, 5733-5779.
2. De Dios, A. C.; Jameson, C. J., Recent Advances in Nuclear Shielding Calculations. In *Annual Reports on NMR Spectroscopy*, Webb, G. A., Ed. Elsevier Ltd.: Burlington, 2012; Vol. 77, pp 1-80.
3. Dračinský, M.; Kaminský, J.; Bouř, P., *J. Chem. Phys.*, 2009, **130**, 094106.
4. Pickard, C. J.; Mauri, F., *Phys. Rev. B*, 2001, **63**, 245101.
5. Harris, R. K.; Hodgkinson, P.; Pickard, C. J.; Yates, J. R.; Zorin, V., *Mag. Res. Chem.*, 2007, **45**, S174-S186.
6. Zheng, A.; Liu, S. B.; Deng, F., *J. Comput. Chem.*, 2009, **30**, 222-235.
7. Dračinský, M.; Bouř, P., *J. Chem. Theory Comput.*, 2010, **6**, 288-299.
8. Perras, F. A.; Bryce, D. L., *J. Phys. Chem. C*, 2012, **116**, 19472-19482.
9. Shao, L. M.; Yates, J. R.; Titman, J. J., *J. Phys. Chem. A*, 2007, **111**, 13126-13132.
10. Willis, B. T. M.; Pryor, A. W., *Thermal Vibrations in Crystallography*. Cambridge University Press: Cambridge, 1975.

11. Apperley, D. C.; Harris, R. K.; Hodgkinson, P., *Solid-State NMR: Basic Principles & Practice*. Momentum Press: New York, 2012.
12. *Nuclear Magnetic Resonance Probes of Molecular Dynamics*. Kluwer Academic Publishers: 1994.
13. Hodgkinson, P., Intramolecular motion in crystalline solids. In *NMR Crystallography*, Harris, R. K.; Wasylshen, R. E.; Duer, M. J., Eds. John Wiley & Sons: Chichester, 2009; pp 375-386.
14. Gervais, C.; Dupree, R.; Pike, K. J.; Bonhomme, C.; Profeta, M.; Pickard, C. J.; Mauri, F., *J. Phys. Chem. A*, 2005, **109**, 6960-6969.
15. Kong, X. Q.; O'Dell, L. A.; Terskikh, V.; Ye, E.; Wang, R. Y.; Wu, G., *J. Am. Chem. Soc.*, 2012, **134**, 14609-14617.
16. Folliet, N.; Roiland, C.; Begu, S.; Aubert, A.; Mineva, T.; Goursot, A.; Selvaraj, K.; Duma, L.; Tielens, F.; Mauri, F.; Laurent, G.; Bonhomme, C.; Gervais, C.; Babonneau, F.; Azais, T., *J. Am. Chem. Soc.*, 2011, **133**, 16815-16827.
17. Ilott, A. J.; Palucha, S.; Batsanov, A. S.; Wilson, M. R.; Hodgkinson, P., *J. Am. Chem. Soc.*, 2010, **132**, 5179-5185.
18. Dumez, J. N.; Pickard, C. J., *J. Chem. Phys.*, 2009, **130**, 104701.
19. Dračinský, M.; Bouř, P., *J. Comput. Chem.*, 2012, **33**, 1080-1089.
20. Griffin, J. M.; Wimperis, S.; Berry, A. J.; Pickard, C. J.; Ashbrook, S. E., *J. Phys. Chem. C*, 2009, **113**, 465-471.
21. Dračinský, M.; Kaminský, J.; Bouř, P., *J. Phys. Chem. B*, 2009, **113**, 14698-14707.
22. Mafra, L.; Santos, S. M.; Siegel, R.; Alves, I.; Paz, F. A. A.; Dudenko, D.; Spiess, H. W., *J. Am. Chem. Soc.*, 2012, **134**, 71-74.
23. Frank, A.; Möller, H. M.; Exner, T. E., *J. Chem. Theor. Comput.*, 2012, **8**, 1480-1492.
24. De Gortari, I.; Portella, G.; Salvatella, X.; Bajaj, V. S.; van der Wel, P. C. A.; Yates, J. R.; Segall, M. D.; Pickard, C. J.; Payne, M. C.; Vendruscolo, M., *J. Am. Chem. Soc.*, 2010, **132**, 5993-6000.
25. Bjornsson, R.; Früchtel, H.; Bühl, M., *Phys. Chem. Chem. Phys.*, 2011, **13**, 619-627.
26. Pennanen, T. S.; Vaara, J.; Lantto, P.; Sillanpaa, A. J.; Laasonen, K.; Jokisaari, J., *J. Am. Chem. Soc.*, 2004, **126**, 11093-11102.
27. Allen, F. H., *Acta Cryst. B*, 2002, **58**, 380-388.
28. Niimura, N.; Arai, S.; Kurihara, K.; Chatake, T.; Tanaka, I.; Bau, R., *Cell. Mol. Life Sci.*, 2006, **63**, 285-300.
29. Clark, S. J.; Segall, M. D.; Pickard, C. J.; Hasnip, P. J.; Probert, M. J.; Refson, K.; Payne, M. C., *Z. Kristallogr.*, 2005, **220**, 567-570.
30. Perdew, J. P.; Burke, K.; Ernzerhof, M., *Phys. Rev. Lett.*, 1996, **77**, 3865-3868.
31. Monkhorst, H. J.; Pack, J. D., *Phys. Rev. B*, 1976, **13**, 5188-5192.
32. Yates, J. R.; Pickard, C. J.; Mauri, F., *Phys. Rev. B*, 2007, **76**, 024401.
33. Vanderbilt, D., *Phys. Rev. B*, 1990, **41**, 7892-7895.
34. Jonsson, P. G.; Kvick, A., *Acta Cryst. B*, 1972, **28**, 1827-1833.
35. Kessler, J.; Dračinský, M.; Bouř, P., *J. Comput. Chem.*, 2013, **34**, 366-371.
36. Netzel, J.; Hofmann, A.; van Smaalen, S., *Crystengcomm*, 2008, **10**, 335-343.
37. Langan, P.; Mason, S. A.; Myles, D.; Schoenborn, B. P., *Acta Cryst. B*, 2002, **58**, 728-733.
38. Webber, A. L.; Elena, B.; Griffin, J. M.; Yates, J. R.; Pham, T. N.; Mauri, F.; Pickard, C. J.; Gil, A. M.; Stein, R.; Lesage, A.; Emsley, L.; Brown, S. P., *Phys. Chem. Chem. Phys.*, 2010, **12**, 6970-6983.
39. Ye, C. H.; Fu, R. Q.; Hu, J. Z.; Hou, L.; Ding, S. W., *Magn. Reson. Chem.*, 1993, **31**, 699-704.
40. Sherwood, M. H.; Alderman, D. W.; Grant, D. M., *J. Magn. Reson. Ser. A*, 1993, **104**, 132-145.
41. Witter, R.; Hesse, S.; Sternberg, U., *J. Magn. Reson.*, 2003, **161**, 35-42.
42. Wu, G.; Dong, S.; Ida, R.; Reen, N., *J. Am. Chem. Soc.*, 2002, **124**, 1768-1777.
43. Pike, K. J.; Lemaitre, V.; Kukul, A.; Anupold, T.; Samoson, A.; Howes, A. P.; Watts, A.; Smith, M. E.; Dupree, R., *J. Phys. Chem. B*, 2004, **108**, 9256-9263.

44. Lemaitre, V.; Pike, K. J.; Watts, A.; Anupold, T.; Samoson, A.; Smith, M. E.; Dupree, R., *Chem. Phys. Lett.*, 2003, **371**, 91-97.